Chemical Engineering Journal 297 (2016) 121–127

Contents lists available at ScienceDirect

Chemical Engineering Journal

journal homepage: www.elsevier.com/locate/cej

A layered-template-nanospace-confinement strategy for production of corrugated graphene nanosheets from petroleum pitch for supercapacitors

Xiaojun He [a,*], Nan Zhang [a], Xiaolong Shao [a], Mingbo Wu [b], Moxin Yu [a], Jieshan Qiu [c,*]

[a] School of Chemistry and Chemical Engineering, Anhui Key Lab of Coal Clean Conversion and Utilization, Anhui University of Technology, No. 59 Hudong Road, Maanshan 243002, China
[b] State Key Lab of Heavy Oil Processing, China University of Petroleum, Qingdao 266580, China
[c] Carbon Research Lab, Liaoning Key Lab for Energy Materials and Chemical Engineering, State Key Lab of Fine Chemicals, Dalian University of Technology, Dalian 116024, China

HIGHLIGHTS

- Corrugated graphene nanosheets (CGNSs) were firstly synthesized from petroleum pitch.
- The specific surface area of CGNSs ranges from 2095 to 2216 $m^2 g^{-1}$.
- The CGNS electrode shows high capacitance, good rate performance and cycle stability.
- This work provides a new way for fabricating low-cost CGNSs for supercapacitors.

GRAPHICAL ABSTRACT

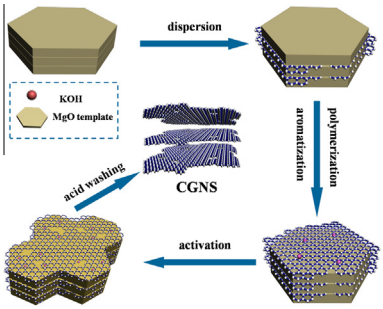

ARTICLE INFO

Article history:
Received 26 January 2016
Received in revised form 30 March 2016
Accepted 31 March 2016
Available online 7 April 2016

Keywords:
Corrugated graphene nanosheets
Petroleum pitch
Layered-template-nanospace-confinement strategy
Supercapacitor

ABSTRACT

Corrugated graphene nanosheets (CGNSs) with abundant short pores for ion transport are highly demanded as one of the most promising electrode materials for high-performance supercapacitors. However, the efficient production of CGNSs remains a big challenge. Herein, a layered-template-nano space-confinement strategy coupled with *in situ* chemical activation is reported to synthesize CGNSs from petroleum pitch. Firstly, petroleum pitch was mixed with potassium hydroxide (KOH) particles, and the mixture was dispersed between and onto the sheet-like nano-MgO templates. Secondly, the nano-MgO templates coated with petroleum pitch and KOH mixture were heated, in which the petroleum pitch was polymerized, leading to interconnected film in the layered-template-confinement-nano space. At the same time, the thin films were activated *in situ* by KOH in the nanospace, and yielding CGNSs after removing the template by acid washing. The thin sheet-like CGNSs feature many wrinkles and hierarchical short pores, and have a high specific surface area up to 2132 $m^2 g^{-1}$ and a big lateral size/thickness aspect ratio. As electrodes for supercapacitors, the CGNSs show a high capacitance of 280 $F g^{-1}$ at 0.05 $A g^{-1}$ in 6 M KOH electrolyte, an excellent rate performance with capacitance remaining at 233 $F g^{-1}$ at 20 $A g^{-1}$ and a superior cycle stability with over 96.8% capacitance retention after 1000 charge–discharge cycles at 1 $A g^{-1}$. This layered-template-nanospace-confinement strategy may pave an efficient way for large scale production of electrode materials from cheap petroleum pitch for high-performance supercapacitors.

* Corresponding authors. Tel.: +86 555 2312355; fax: +86 555 2311822 (X. He).
Tel.: +86 411 84986080; fax: +86 411 84986015 (J. Qiu).
E-mail addresses: agdxjhe@126.com (X. He), jqiu@dlut.edu.cn (J. Qiu).

http://dx.doi.org/10.1016/j.cej.2016.03.153
1385-8947/

1. Introduction

The limited availability of fossil fuels in the long run has prompted the exploration and utilization of sustainable energy resources such as solar energy and wind energy. For the sake of efficient utilization of these resources, energy storage devices that can effectively store and release the electrical energy on demand are highly required. Among the energy storage devices, supercapacitors have attracted increasing attention in recent years in view of their rapid charge–discharge rate, high power density and long cycle life. The electrochemical performance of supercapacitors depends on the electrode materials largely [1]. Various carbon materials, such as activated carbons [2], carbon fibers [3], carbon nanotubes/activated carbons [4], mesoporous carbons [5], carbon nanocages/nanospheres [6], carbon nanotubes [7], and graphene [8,9] have been widely investigated as electrode materials for supercapacitors. Among them, graphene, a two-dimensional carbon material, is one of the most promising electrode candidates for supercapacitors owing to its high theoretical surface area, good electric conduction and electrochemical stability [10]. However, graphene nanosheets tend to agglomerate in an irreversible way or restack due to van der Waals interactions between the sheets, resulting in the loss of the specific surface area and lowered specific capacitance thereafter. Therefore, efforts have been made to tackle this problem, such as the design of sandwich-like structures with metal oxides or carbon nanomaterials as "spacers" between the sheets [11,12], the development of graphene foams [13], and three-dimensional porous graphene [14]. Nevertheless, the methods available now for the synthesis of less-stacked graphene nanosheets are time- and energy-consuming, leading to the high-cost of the graphene materials. Therefore, it is necessary to develop an efficient method for production of corrugated graphene nanosheets (CGNSs) with abundant short pores that are easily accessible to ions, which is helpful for fast ion transport and for delivering excellent supercapacitance.

Petroleum pitch, a residue from the distillation of crude oils in petrochemical industry, is cheap and abundant. The aromatic hydrocarbons are abundant in petroleum pitch, featuring sp^2-hybridized carbon atoms, and are highly similar to the hexagonally ranged carbon atoms in graphene. These aromatic hydrocarbon molecules in petroleum pitch may be polymerized and further aromatized to large interconnected thin polymeric films in the layered-template-confinement-nanospace, and the thin polymer films can be further transformed into graphene nanosheets in the nanospace at high temperatures.

Herein, we report a layered-template-nanospace-confinement strategy coupled with *in situ* chemical activation to synthesize CGNS from petroleum pitch. Petroleum pitch mixed with KOH particles was firstly dispersed between the sheet-like MgO templates, where the aromatic hydrocarbon molecules in petroleum pitch undergo a polymerization step to thin films in the layere d-template-confinement-nanospace. The resultant thin films were then converted into CGNSs by high temperature annealing. The CGNS materials were finally obtained after removing the template via acid washing. The thin CGNS materials are found to have abundant hierarchical short pores and large sheets. This kind of pores are favorable for ion adsorption, and for fast ion transport, and the large sheets favor the fast electron conduction, which combine to result in improved supercapacitance. To the best of our knowledge, reports on the high-efficiency synthesis of such unique CGNSs from petroleum pitch for supercapacitors have not been reported.

2. Experimental

2.1. Synthesis of CGNSs

Petroleum pitch was obtained from CNOOC (China National Offshore Oil Corp.) with 87.39 wt% of carbon, 7.93 wt% of hydrogen, 3.30 wt% of sulfur, 1.30 wt% of nitrogen and 0.07 wt% of oxygen. Other chemicals were purchased from Aladdin without further purification. In a typical run, petroleum pitch with a particle size below 100 μm (3.0 g), sheet-like nano-MgO (18.0 g) and KOH (6.0 g) were ground, respectively, and mixed in solid state. The resultant mixtures were transferred to a corundum boat, which was put into a tube furnace and heated to 473 K at 5 K min^{-1}, and kept for 30 min in flowing argon of 60 mL min^{-1}, then heated to 1073 K at 5 K min^{-1} and kept for 1 h to make CGNSs. The CGNSs were obtained by acid washing with 2 M HCl solution and distilled water repeatedly to remove the template and inorganic impurities. The as-made CGNS is termed as $CGNS_{3\text{-}1073}$, where the subscript 3 refers to the mass of petroleum pitch, and 1073 is the heat treatment temperature. Similarly, CGNS made at 1073 K for 1 h with 2.0 g petroleum pitch, 19.0 g MgO, 6.0 g KOH is termed as $CGNS_{2\text{-}1073}$, and CGNS made at 1173 K for 1 h with the mass of petroleum pitch, MgO, KOH at 3.0 g, 18.0 g, 6.0 g is termed as $CGNS_{3\text{-}1173}$ with other conditions remaining unchanged.

2.2. Characterization of CGNS

The CGNS materials and MgO were examined by transmission electron microscopy (TEM, JEOL-2100), scanning electron microscopy (SEM, S-4800), and X-ray photoelectron spectroscopy (XPS, Thermo ESCALAB250, USA) to reveal the chemical bonding states of carbon and oxygen elements in CGNSs. The Raman spectra of CGNSs were recorded on a Raman spectroscopy (JYLab−Ram HR800, excited by a 532 nm laser). The water contact angle of the samples was measured by the contact angle measurement system (OCA15Pro, DataPhysics Instruments, Germany). The electrical conductivity of the CGNS materials was measured on a GM-II multifunction automatic measuring instrument. The CGNS materials were pressed into a thin disk at 30 MPa cm^{-2}. Nitrogen adsorption–desorption isotherms were obtained at 77 K with an Autosorb-IQ system (Quantachrome, USA). The surface area (S_{BET}) of CGNSs was calculated by the BET method. The pore size distribution was calculated by the density functional theory (DFT) method from the adsorption branches of the isotherms. The total pore volume (V_t) was estimated at $P/P_0 = 0.99$, and the micropore volume (V_{mic}) was estimated using the *t*-plot method. The non-V_{mic} was calculated from the difference of V_t and V_{mic}. The average pore size (D_{ap}) of CGNSs was obtained by the equation of $D_{ap} = 4V_t/S_{BET}$.

2.3. Preparation and electrochemical test of CGNS electrodes

The electrochemical properties of the as-obtained CGNS materials were investigated using two-electrode cell at room temperature. The electrodes were prepared by mixing 88.0 wt% of CGNSs and 12.0 wt% of polytetrafluoroethylene (PTFE), and then rolled into carbon film and cut into a round film with a diameter of 12 mm, which was further dried at 383 K for 2 h under vacuum. The resultant carbon film was pressed onto nickel foam to make supercapacitor electrodes. Before the electrochemical test, the electrodes was soaked overnight in 6 M KOH aqueous electrolyte. The button-type supercapacitor was assembled with two similar electrodes (about 2.1 mg cm^{-2}) separated by a polypropylene

membrane. The supercapacitors were evaluated by cyclic voltammetry (CV) at the sweep rates from 2 to 500 mV s^{-1} at room temperature. The cut off charge voltage for supercapacitor in 6 M KOH aqueous electrolyte was operated at a range of 0–1 V. Electrochemical impedance spectroscopy (EIS) measurement was performed with an amplitude of 5 mV over a frequency of 100 kHz to 0.001 Hz using a Solartron impedance analyzer (Solartron Analytical, SI 1260, UK) with a Solartron potentiostat (SI 1287). The galvanostatic charge–discharge measurement was performed on a supercapacitance test system (SCTs, Arbin Instruments, USA). The gravimetric capacitance of the single CGNS electrode, C (F g^{-1}), was calculated from the galvanostatic discharge process according to Eq. (1).

$$C = \frac{4I}{m\frac{\Delta V}{\Delta t}} \tag{1}$$

where I is the discharge current (A), ΔV is the discharge voltage (V) between the Δt discharge time (s), and m is the total mass of the active material for both electrodes (g).

The energy density (E, W h kg^{-1}) and average power density (P, W kg^{-1}) of the supercapacitors were obtained according to Eqs (2) and (3).

$$E = \frac{1}{2 \times 4 \times 3.6} CV^2 \tag{2}$$

$$P = \frac{E}{\Delta_{td}} \tag{3}$$

where V is the usable voltage after the IR drop (V), and Δ_{td} is the discharge time (h).

3. Results and discussion

Fig. 1 shows the TEM images of sheet-like MgO particles and CGNSs. Fig. 1a is the sheet-like image of nano-MgO templates, inset is the SEM image. Fig. 1b is the TEM image of unwashed $CGNS_{3\text{-}1073}$ that contains sheet-like MgO. The thin carbon layer can be observed at the edge of MgO templates, as shown in the inset in Fig. 1b. All the graphene images in Fig. 1c–e are transparent to electron beams, demonstrating that they are extremely thin due to the confined growth of CGNSs in the layered-MgO-template-confine ment-nanospace. Fig. 1c is the TEM image of $CGNS_{3\text{-}1073}$, in which many wrinkles in the thin graphene sheets can be seen, which may help to prevent the loss of surface-area and allow quick ion transport across the electrodes, resulting in an improved capacitance by forming more ion paths. The thin graphene sheets are expected to improve the rate performance due to the shortened transport distance of ions in the short pores. Fig. 1d and e are the TEM images of $CGNS_{2\text{-}1073}$ and $CGNS_{3\text{-}1173}$, respectively. Different from the morphology of $CGNS_{3\text{-}1073}$ in Fig. 1c, many macropores can be observed

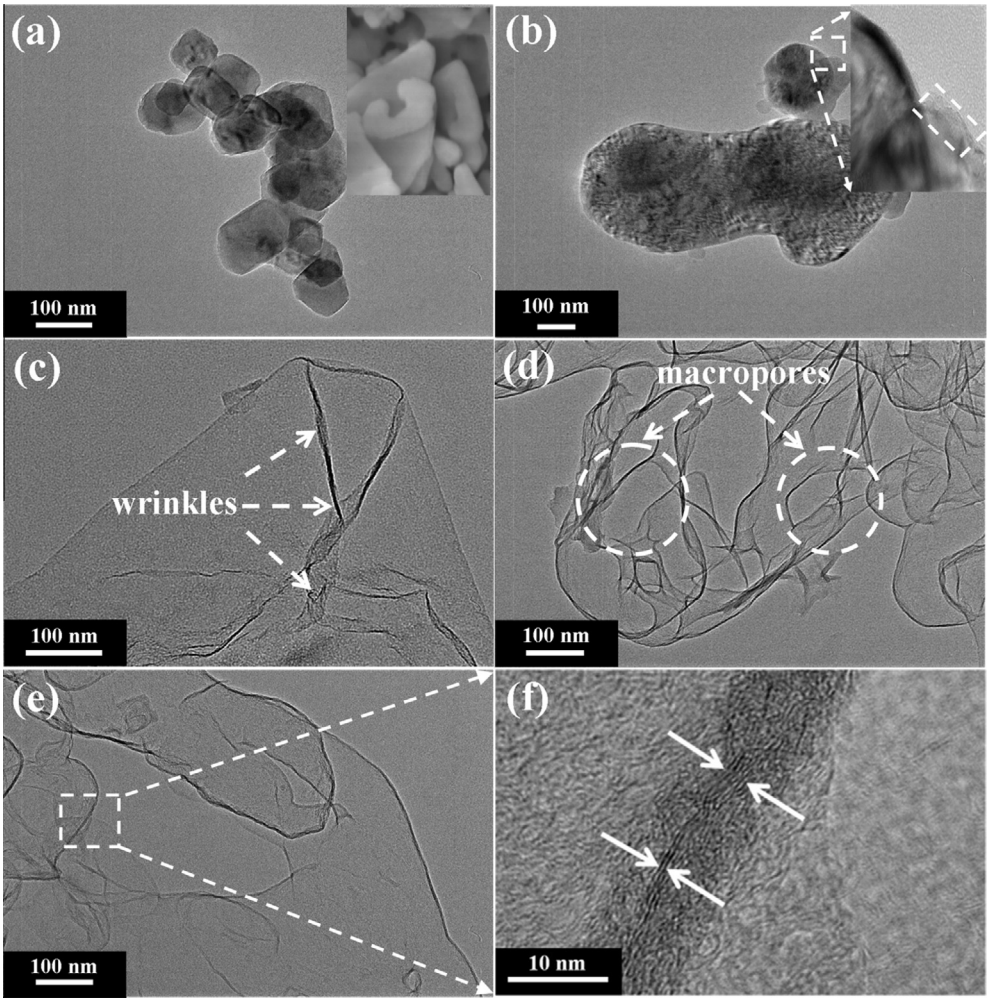

Fig. 1. TEM images of (a) sheet-like MgO particles, inset is the SEM image, (b) unwashed $CGNS_{3\text{-}1073}$, (c) $CGNS_{3\text{-}1073}$, (d) $CGNS_{2\text{-}1073}$, (e) $CGNS_{3\text{-}1173}$, (f) high resolution TEM image of the shell of $CGNS_{3\text{-}1173}$.

in $CGNS_{2\text{-}1073}$ and $CGNS_{3\text{-}1173}$, indicating that higher alkali dosage and higher calcination temperature result in more macropores. Obviously, the morphology of CGNSs can be adjusted by changing the mass of raw materials, or the calcination temperature. The TEM image in Fig. 1f shows that the graphene in $CGNS_{3\text{-}1173}$ has 2–6 layers, indicative of extremely thin thickness of the CGNSs. Usually, the undamaged graphene sheets are expected to improve electron conduction. The electrical conductivity of $CGNS_{3\text{-}1073}$, $CGNS_{2\text{-}1073}$, $CGNS_{3\text{-}1173}$ is 385, 244, 185 S m^{-1}. The highest electrical conductivity of $CGNS_{3\text{-}1073}$ is ascribed to its perfect sheet-like structure, as shown in Fig. 1c.

Based on the TEM images in Fig. 1, one can envision the schematic of direct fabrication process of CGNSs from petroleum pitch, as shown in Fig. 2. Firstly, petroleum pitch with aromatic hydrocarbons mixed with KOH particles is uniformly dispersed between the layered-MgO-template-confinement-nanospace. The MgO sheets with layered nanospace function as a nano-template or nano-reactor to confine and modulate the transformation of petroleum pitch. The polymerization reactions of active free radicals among the carbon atoms of the neighboring aromatic rings will take place, yielding interconnected thin polymer films made of aromatic benzene-like rings. Secondly, the as-formed polymer films in the nanospace are further heated, leading to graphene sheets with abundant hierarchical pores that are created due to the *in situ* activation of the embedded KOH at elevated temperatures. Finally, the CGNSs are obtained after removing the template by repeated washing with 2 M HCl solution and distilled water.

The nitrogen adsorption–desorption isotherms of the CGNSs shown in Fig. 3a are typical IV type with strong N_2 adsorption at low pressure and obvious loops at relative pressure of 0.5−1.0, indicating the presence of micropores and mesopores in the CGNS samples. Fig. 3b shows the pore size distribution of the CGNS materials. The pore size of $CGNS_{3\text{-}1173}$ and $CGNS_{2\text{-}1073}$ ranges from 0.70 to 3.0 nm, and from 0.80 to 3.0 nm, respectively. The micropores of $CGNS_{3\text{-}1073}$ are only in the range of 0.50−2.0 nm. As shown in Fig. 3b, there are some smaller micropores in $CGNS_{3\text{-}1073}$ in comparison to bigger micropores in $CGNS_{3\text{-}1173}$ and $CGNS_{2\text{-}1073}$. This illustrates that higher alkali dosage or higher calcination temperature facilitate the formation of bigger micropores because some smaller micropores are widened and incorporated into mesopores and macropores, evidenced by the TEM images in Fig. 1d and e. The pore structure parameters of CGNS samples are summarized in Table 1. The D_{ap} of CGNSs increases from 2.30 nm ($CGNS_{3\text{-}1073}$) to 2.40 nm ($CGNS_{2\text{-}1073}$) when the dosage of petroleum pitch in the reactants drops from 3.0 g to 2.0 g while the MgO dosage increases from 18.0 to 19.0 g with other conditions remaining unchanged. The S_{BET} of $CGNS_{3\text{-}1173}$ reaches 2216 m^2 g^{-1}, which is slightly higher than that of $CGNS_{3\text{-}1073}$ (2132 m^2 g^{-1}). The yields of three CGNS samples are higher than 44.6%, indicating high synthesis efficiency. The above results indicate that the pore structure of the CGNSs can be adjusted by changing the mass ratio of reactants and the calcination temperature. Fig. 3c presents the Raman spectra of CGNSs, showing the D-band at ~1320 cm^{-1} due to the breathing mode of aromatic rings and G-band at ~1590 cm^{-1} associated with the bond stretching of sp^2 carbon [15]. The peak intensity ratio (I_D/I_G) of $CGNS_{3\text{-}1073}$ is only 0.84, which is smaller than that of wrinkled carbon nanotubes, indicative of a higher graphitization degree [16]. The intense D-band indicates the partial lattice defects owing to abundant pores compared to single graphene layer. This result is consistent with the typical Raman spectra of graphene oxide and reduced graphene oxides [8,9]. Fig. 3d is the XPS spectra of the CGNSs, showing that no impurities are observed in CGNSs except the C1s and O1s peaks. The O1 s peaks can be deconvoluted into oxygen-containing groups C═O (531.9 eV), C—O (533.4 eV), and O—H, as shown in inset in Fig. 3d. Oxygen functional groups can improve the wettability of electrode materials in electrolytes, depending on their hydrophilic nature, which can also prevent the aggregation of adjacent graphene sheets [17]. The contents of surface oxygen-containing functional groups of the CGNSs are summarized in Table 2. The results of water contact angle measurement in Fig. 3e show that the initial contact angle of $CGNS_{3\text{-}1073}$, $CGNS_{2\text{-}1073}$, $CGNS_{3\text{-}1173}$ is 46.2, 84.2, 64.7 degree, respectively. The $CGNS_{3\text{-}1073}$ with more hydrophilic oxygen-containing functional groups has the smallest contact angle, implying its best wettability with the electrolyte, as shown in Table 2.

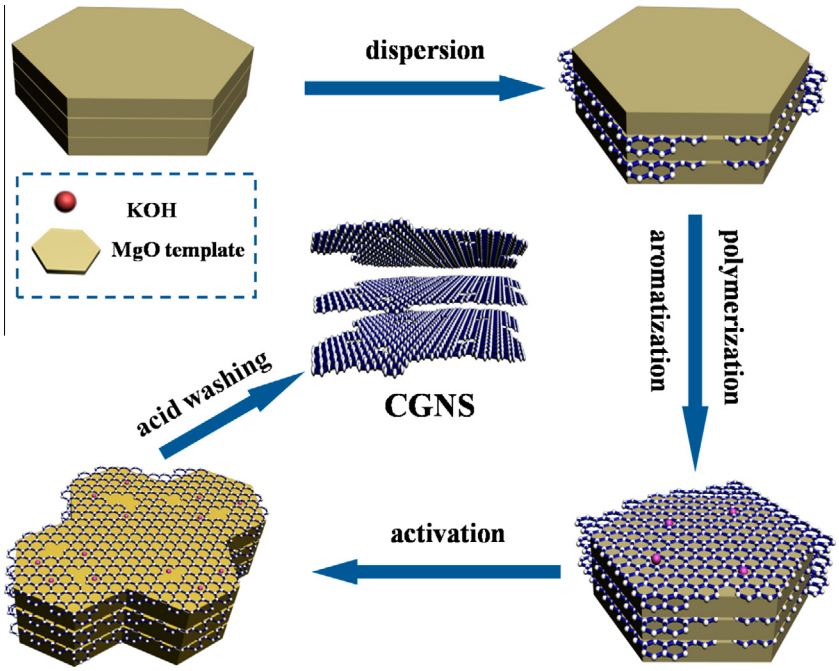

Fig. 2. Schematic of direct fabrication process of CGNSs from petroleum pitch.

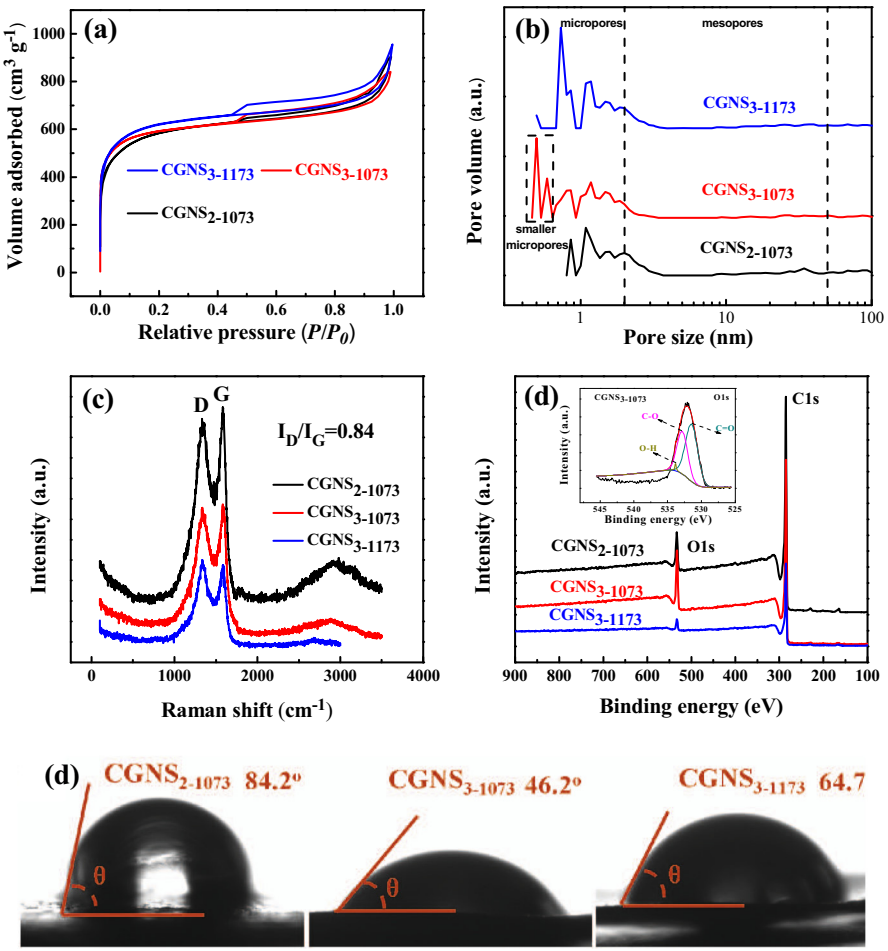

Fig. 3. (a) Nitrogen adsorption–desorption isotherms of CGNSs; (b) pore size distribution of CGNSs; (c) Raman spectra of CGNSs; (d) XPS spectra of CGNSs; (e) the water contact angle of CGNSs.

Table 1
The pore structure parameters of CGNSs.

CGNS samples	D_{ap} (nm)	S_{BET} ($m^2\ g^{-1}$)	S_{mic} ($m^2\ g^{-1}$)	V_t ($cm^3\ g^{-1}$)	V_{mic} ($cm^3\ g^{-1}$)	non-V_{mic} ($cm^3\ g^{-1}$)
$CGNS_{2\text{-}1073}$	2.40	2095	1878	1.26	0.85	0.41
$CGNS_{3\text{-}1073}$	2.30	2132	1920	1.23	0.84	0.39
$CGNS_{3\text{-}1173}$	2.31	2216	2024	1.28	0.91	0.37

Table 2
The quantity of surface oxygen-containing functional groups of CGNSs.

CGNS samples	C1s (%)	O1s (%)	O1s		
			C=O (%)	C–O (%)	O–H (%)
$CGNS_{2\text{-}1073}$	83.4	16.3	7.6	6.1	2.6
$CGNS_{3\text{-}1073}$	74.8	25.2	15.1	9.8	0.3
$CGNS_{3\text{-}1173}$	84.4	15.6	8.1	6.1	1.4

Fig. 4a shows the specific capacitance of CGNS electrodes in 6 M KOH aqueous electrolyte at different current densities. The specific capacitance of $CGNS_{3\text{-}1073}$ electrodes reaches 280 F g^{-1} at 0.05 A g^{-1} and retains 233 F g^{-1} at 20 A g^{-1} with a capacitance retention of 83.2%, showing the highest capacitance and best rate performance, which may be due to its biggest electrical conductivity and best wettability with the electrolyte. The rich micropores (e.g. from 0.5 to 2.0 nm) in $CGNS_{3\text{-}1073}$ electrodes may be utilized since the size of hydrated cations and anions in 6 M KOH aqueous electrolyte is only 0.26 and 0.15 nm, respectively. Considering the thin thickness and the pore size of the CGNSs, one can work out that the ratio of pore length to pore size of CGNSs is below 10. Such a small ratio ensures that the abundant micropores in CGNSs are accessible for fast ion adsorption and desorption, which renders high capacitance and excellent rate performance. Fig. 4b presents the comparison of specific capacitance and current density of $CGNS_{3\text{-}1073}$ electrodes with other electrodes in aqueous electrolytes. The capacitance of $CGNS_{3\text{-}1073}$ electrodes is higher than those reported in literature [18–32]. The high capacitance and rate performance of $CGNS_{3\text{-}1073}$ electrodes are ascribed to the excellent conduction of graphene nanosheets for electrons, short pores in thin graphene nanosheets for fast ion transport, and abundant accessible micropores together with considerable wrinkles for ion adsorption. Fig. 4c presents the cycle performance of $CGNS_{3\text{-}1073}$ electrodes, showing a high capacitance retention of 96.8% after 1000 charge–discharge cycles at 1 A g^{-1}. The inset in Fig. 4c shows that the galvanostatic charge–discharge curve of $CGNS_{3\text{-}1073}$

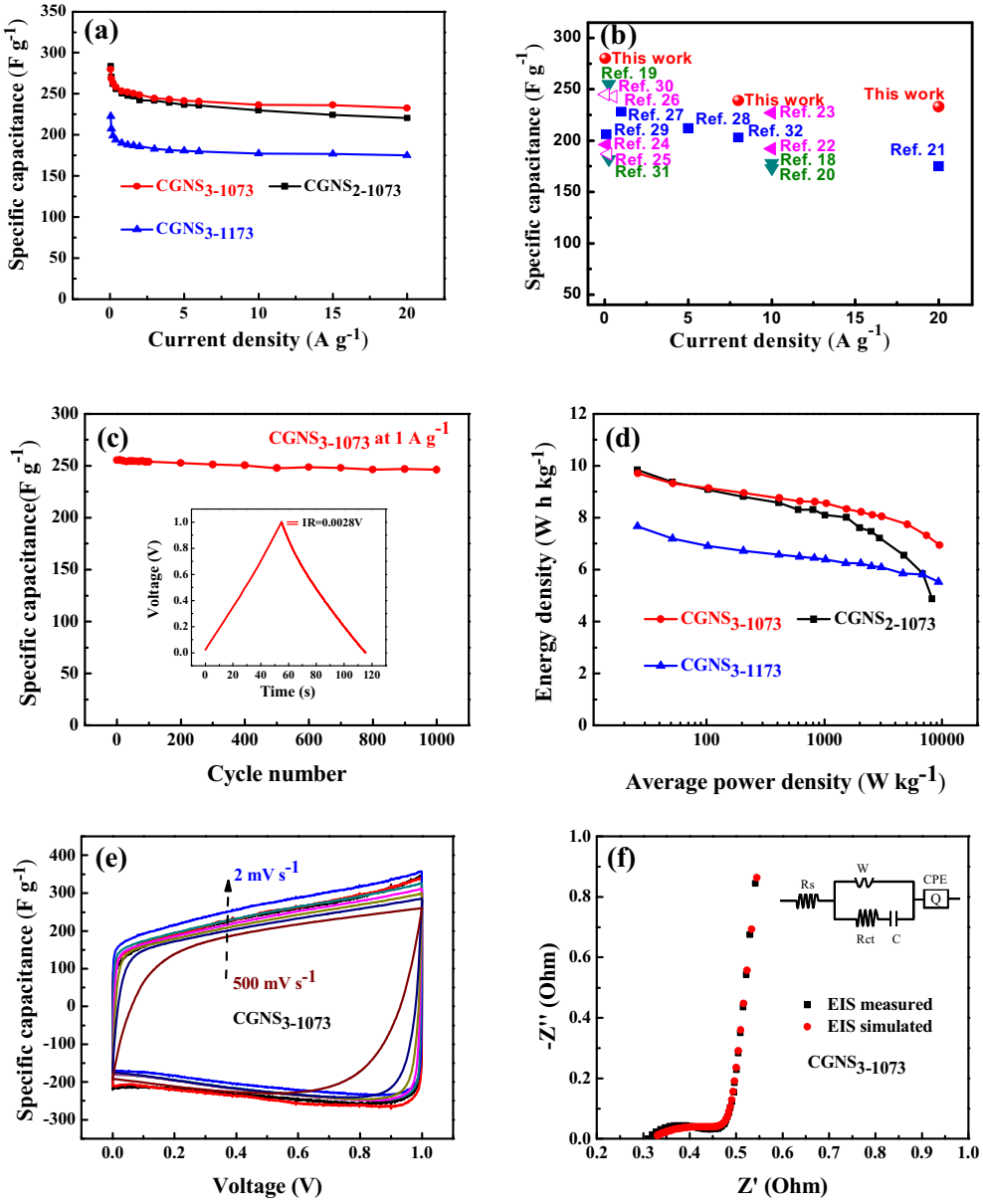

Fig. 4. (a) Specific capacitance of CGNS electrodes at different current densities; (b) comparison of specific capacitance and current density of $CGNS_{3\text{-}1073}$ electrodes with other electrodes in aqueous electrolytes; (c) cycle stability of $CGNS_{3\text{-}1073}$ electrodes measured at 1.0 A g^{-1}, inset is the charge–discharge curve; (d) Ragone plots of CGNS capacitors; (e) CV curves of $CGNS_{3\text{-}1073}$ electrodes at different scan rates; (f) Nyquist plots of $CGNS_{3\text{-}1073}$ electrodes.

electrodes is symmetrical without obvious pseudocapacitance behavior at 1.0 A g^{-1} in 6 M KOH aqueous electrolyte, which is the typical characteristics of ideal supercapacitors. The IR drop of $CGNS_{3\text{-}1073}$ is only 0.0028 V at current density of 1.0 A g^{-1}, indicating that the CGNS electrodes have very small internal resistance. The above good electrochemical properties are partly ascribed to the micro-meso-macropores in CGNSs, which function as active sites for ion adsorption and transport. The CGNSs combine the advantages of high utilization of micropores in the hierarchical porous structure, high conductivity and lateral size/thickness aspect ratio for electron conduction, and short pores for fast ion transport. Fig. 4d shows the Ragone plots of CGNS electrodes in 6 M KOH aqueous electrolyte. The energy density of $CGNS_{3\text{-}1073}$ capacitor reaches 9.70 W h kg^{-1} at 0.05 A g^{-1} and 6.94 W h kg^{-1} at 20 A g^{-1}, with the energy density retention of 71.5%. The high energy retention of $CGNS_{3\text{-}1073}$ capacitor is attributed to the highest electrical conductivity and the best wettability as well as the corrugated sheet-like structure to prevent the graphene nanosheets from agglomeration and sheet-to-sheet restacking. Fig. 4e is the CV curves of $CGNS_{3\text{-}1073}$ electrodes at different scan rates. The good quasi-rectangular shapes without obvious redox peaks indicate ideal capacitive behavior. Even at high scan rate of 500 mV s^{-1}, the CV curve still retain quasi-rectangular shape without obvious distortion, proving the excellent rate performance of $CGNS_{3\text{-}1073}$ electrode and the formation of perfect electrical double layers due to the reversible adsorption and desorption of the electrolyte ions. Fig. 4f is the Nyquist plots of $CGNS_{3\text{-}1073}$ electrodes, in which the inset is the equivalent circuit model of CGNS electrodes that helps to explain the characteristics of EIS as that reported in our previous work [33]. The short *x*-intercept (0.3 Ohm), negligible diameter of the semicircle and high slope at low frequency reveal that the $CGNS_{3\text{-}1073}$ electrodes have very low internal resistance, charge–discharge resistance and excellent pore accessibility for the electrolyte ions.

The excellent performance of the CGNS electrodes are due to three factors. (i) the interconnected graphene nanosheets in the CGNSs provide nearly perfect substrate for fast electron movement, evidenced by the small IR drop of $CGNS_{3\text{-}1073}$ electrodes that is only 0.0028 V at 1.0 A g^{-1}. (ii) The well-developed pores together with many wrinkles on the thin sheets of the CGNSs provide abundant active sites for ion adsorption, evidenced by the high capacitance. (iii) Short pores through the thin sheets function as fast paths for ion transport, evidenced by the excellent rate performance. To bear in mind, these CGNSs can be conveniently synthesized from cheap petroleum pitch, thus, hold promise as electrodes for high performance supercapacitors.

4. Conclusions

Novel CGNSs have been synthesized for the first time directly from petroleum pitch by a layered-MgO-template-nanospace-confinement strategy coupled with *in situ* KOH activation. It is efficient to make the aromatic hydrocarbons in petroleum pitch to be polymerized first, and then converted to interconnected corrugated graphene nanosheets in the layered-template-confinement-nano space. The as-made CGNSs feature abundant pores for ion adsorption, short pores for ion transport and interconnected graphene nanosheets for electron conduction. Because of these structural merits, the CGNS electrodes show high capacitance of 280 F g^{-1} in 6 M KOH aqueous electrolyte, excellent rate performance of 233 F g^{-1} at 20 A g^{-1} and superior cycle stability with 96.8% of capacitance retention after 1000 cycles at 1.0 A g^{-1}. This novel strategy may pave a way for efficient synthesis of low-cost graphene materials for supercapacitors from aromatic hydrocarbon sources such as petroleum pitch that need to be utilized for added-value carbon materials.

Acknowledgments

This work was partly supported by the NSFC (Nos. 51272004 and U1361110), and the Program for New Century Excellent Talents of the Education Ministry of China (No. NCET-13-0643).

Reference

[1] G.P. Wang, L. Zhang, J.J. Zhang, A review of electrode materials for electrochemical supercapacitors, Chem. Soc. Rev. 41 (2012) 797–828.
[2] J.L. Chang, Z.Y. Gao, X.R. Wang, D.P. Wu, F. Xu, X. Wang, Y.M. Guo, K. Jiang, Activated porous carbon prepared from paulownia flower for high performance supercapacitor electrodes, Electrochim. Acta 157 (2015) 290–298.
[3] Z. Jin, X.D. Yan, Y.H. Yu, G.J. Zhao, Sustainable activated carbon fibers from liquefied wood with controllable porosity for high-performance supercapacitors, J. Mater. Chem. A 2 (2014) 11706–11715.
[4] X. Geng, L.X. Li, F. Li, Carbon nanotubes/activated carbon hybrid with ultrahigh surface area for electrochemical capacitors, Electrochim. Acta 168 (2015) 25–31.
[5] X.J. He, P.H. Ling, J.S. Qiu, M.X. Yu, X.Y. Zhang, C. Yu, M.D. Zheng, Efficient preparation of biomass-based mesoporous carbons for supercapacitors with both high energy density and high power density, J. Power Sources 240 (2013) 109–113.
[6] J. Zhao, H.W. Lai, Z.Y. Lyu, Y.F. Jiang, K. Xie, X.Z. Wang, Q. Wu, L.J. Yang, Z. Jin, Y. W. Ma, J. Liu, Z. Hu, Hydrophilic hierarchical nitrogen-doped carbon nanocages for ultrahigh supercapacitive performance, Adv. Mater. 27 (2015) 3541.
[7] Z.Q. Wang, Z.Q. Wu, G.D. Benedetto, J.L. Zunino, S. Mitra, Microwave synthesis of highly oxidized and defective carbon nanotubes for enhancing the performance of supercapacitors, Carbon 91 (2015) 103–113.
[8] H. Yang, S. Kannappan, A.S. Pandian, J.H. Jang, Y.S. Lee, W. Lu, Nanoporous graphene materials by low-temperature vacuum-assisted thermal process for electrochemical energy storage, J. Power Sources 284 (2015) 146–153.
[9] J. Yan, J.P. Liu, Z.J. Fan, T. Wei, L.J. Zhang, High-performance supercapacitor electrodes based on highly corrugated graphene sheets, Carbon 50 (2012) 2179.
[10] J. Liu, Charging graphene for energy, Nat. Nanotechnol. 9 (2014) 739–740.
[11] D.Y. Zhai, B.H. Li, H.D. Du, G.Y. Gao, L. Gan, Y.B. He, Q.H. Yang, F.Y. Kang, The preparation of graphene decorated with manganese dioxide nanoparticles by electrostatic adsorption for use in supercapacitors, Carbon 50 (2012) 5034–5043.
[12] L.L. Jiang, L.Z. Sheng, C.L. Long, Z.J. Fan, Densely packed graphene nanomesh-carbon nanotube hybrid film for ultra-high volumetric performance supercapacitors, Nano Energy 11 (2015) 471–480.
[13] J.L. Liu, L.L. Zhang, H.B. Wu, J.Y. Lin, Z.X. Shen, X.W. Lou, High-performance flexible asymmetric supercapacitors based on a new graphene foam/carbon nanotube hybrid film, Energy Environ. Sci. 7 (2014) 3709–3719.
[14] X.J. He, H.B. Zhang, H. Zhang, X.J. Li, N. Xiao, J.S. Qiu, Direct synthesis of 3D hollow porous graphene balls from coal tar pitch for high performance supercapacitors, J. Mater. Chem. A 2 (2014) 19633–19640.
[15] Y. Fang, Y.Y. Lv, R.C. Che, H.Y. Wu, X.H. Zhang, D. Gu, G.F. Zheng, D.Y. Zhao, Two-dimensional mesoporous carbon nanosheets and their derived graphene nanosheets: synthesis and efficient lithium ion storage, J. Am. Chem. Soc. 135 (2013) 1524–1530.
[16] G.Q. Ning, C.G. Xu, X. Zhu, R.F. Zhang, W.Z. Qian, F. Wei, Z.J. Fan, J.S. Gao, MgO-catalyzed growth of *N*-doped wrinkled carbon nanotubes, Carbon 56 (2013) 38–44.
[17] Z.Y. Lin, Y. Liu, Y.G. Yao, O.J. Hildreth, Z. Li, K. Moon, C.P. Wong, Superior capacitance of functionalized graphene, J. Phys. Chem. C 115 (2011) 7120–7125.
[18] K. Xie, X.T. Qin, X.Z. Wang, Y.N. Wang, H.S. Tao, Q. Wu, L.J. Yang, Z. Hu, Carbon nanocages as supercapacitor electrode materials, Adv. Mater. 24 (2012) 347–352.
[19] A.M. Abdelkader, Electrochemical synthesis of highly corrugated graphene sheets for high performance supercapacitors, J. Mater. Chem. A 3 (2015) 8519–8525.
[20] L. Hao, B. Luo, X.L. Li, M.H. Jin, Y. Fang, Z.H. Tang, Y.Y. Jia, M.H. Liang, A. Thomas, J.H. Yang, L.J. Zhi, Terephthalonitrile-derived nitrogen-rich networks for high performance supercapacitors, Energy Environ. Sci. 5 (2012) 9747–9751.
[21] M. Oschatz, L. Borchardt, K. Pinkert, S. Thieme, M.R. Lohe, C. Hoffmann, M. Benusch, F.M. Wisser, C. Ziegler, L. Giebeler, M.H. Rümmeli, J. Eckert, A. Eychmüller, S. Kaskel, Hierarchical carbide-derived carbon foams with advanced mesostructure as a versatile electrochemical energy-storage material, Adv. Energy Mater. 4 (2014) 1300645.
[22] L. Qie, W.M. Chen, H.H. Xu, X.Q. Xiong, Y. Jiang, F. Zou, X.L. Hu, Y. Xin, Z.L. Zhang, Y.H. Huang, Synthesis of functionalized 3D hierarchical porous carbon for high-performance supercapacitors, Energy Environ. Sci. 6 (2013) 2497–2504.
[23] W.J. Qian, F.X. Sun, Y.H. Xu, L.H. Qiu, C.H. Liu, S.D. Wang, F. Yan, Human hair-derived carbon flakes for electrochemical supercapacitors, Energy Environ. Sci. 7 (2014) 379–386.
[24] H.J. Wang, X.X. Sun, Z.H. Liu, Z.B. Lei, Creation of nanopores on graphene planes with MgO template for preparing high-performance supercapacitor electrodes, Nanoscale 6 (2014) 6577–6584.
[25] W.F. Zhang, Z.H. Huang, C.J. Zhou, G.P. Cao, F.Y. Kang, Y.S. Yang, Porous carbon for electrochemical capacitors prepared from a resorcinol/formaldehyde-based organic aquagel with nano-sized particles, J. Mater. Chem. 22 (2012) 7158–7163.
[26] F. Gao, G.H. Shao, J.Y. Qu, S.Y. Lv, Y.Q. Li, M.B. Wu, Tailoring of porous and nitrogen-rich carbons derived from hydrochar for high-performance supercapacitor electrodes, Electrochim. Acta 155 (2015) 201–208.
[27] X.M. Fan, C. Yu, J. Yang, Z. Ling, C. Hu, M.D. Zhang, J.S. Qiu, A layered-nanospace-confinement strategy for the synthesis of two-dimensional porous carbon nanosheets for high-rate performance supercapacitors, Adv. Energy Mater. 5 (2015) 1401761.
[28] Y. Guo, Z.Q. Shi, M.M. Chen, C.Y. Wang, Hierarchical porous carbon derived from sulfonated pitch for electrical double layer capacitors, J. Power Sources 252 (2014) 235–243.
[29] J.Y. Qu, C. Geng, S.Y. Lv, G.H. Shao, S.Y. Ma, M.B. Wu, Nitrogen, oxygen and phosphorus decorated porous carbons derived from shrimp shells for supercapacitors, Electrochim. Acta 176 (2015) 982–988.
[30] W. Lin, B. Xu, L. Liu, Hierarchical porous carbon prepared by NaOH activation of nano-$CaCO_3$ templated carbon for high rate supercapacitors, New J. Chem. 38 (2014) 5509–5514.
[31] H.J. Wang, L. Zhi, K.Q. Liu, L.Q. Dang, Z.H. Liu, Z.B. Lei, C. Yu, J.S. Qiu, Thin-sheet carbon nanomesh with an excellent electrocapacitive performance, Adv. Funct. Mater. 25 (2015) 5420–5427.
[32] J.L. Huang, J.Y. Wang, C.W. Wang, H.N. Zhang, C.X. Lu, J.Z. Wang, Hierarchical porous graphene carbon-based supercapacitors, Chem. Mater. 27 (2015) 2107–2113.
[33] X.J. He, Y.J. Geng, J.S. Qiu, M.D. Zheng, S.A. Long, X.Y. Zhang, Effect of activation time on the properties of activated carbons prepared by microwave-assisted activation for electric double layer capacitors, Carbon 48 (2010) 1662–1669.